Surface heterogeneity in KTaO₃ (001)

Pratik Koirala*, Ahmet Gulec, Laurence D. Marks

Department of Materials Science and Engineering, Northwestern University, Evanston, IL 60208, USA

ABSTRACT

Surface heterogeneity in Ar^+ ion bombarded samples of (001) oriented $KTaO_3$ was studied using (in-situ) electron microscopy and atomic force microscopy. Ion bombardment results in surface damage as well as in off-stoichiometry of K and Ta due to the large differences in atomic radii of the two constituent elements and hence different dry etching rates. Subsequent annealing of such samples reduces the potassium content via vaporization and results in the formation of tantalum-rich secondary phases on the surface. The phase that segregates on the surface is dependent on the oxygen partial pressure, annealing temperature as well as K:Ta stoichiometry. However, samples etched with chemical means to remove lattice damage and surface disorder prior to annealing exhibit little to no surface heterogeneity.

1. Introduction

In recent years there has been substantial interest in perovskites materials for thin film growth, electronics, catalysis and other applications. Potassium tantalate ($KTaO_3$) has received significant interest due to its remarkable dielectric property that monotonically increases to a value of about 4500 at liquid He temperatures [1]. It also exhibits a two-dimensional electron at its interface with $LaTiO_3$ [2]. A wide range of other applications in catalysis [3,4], tunable microwave devices [1], air treatment [5] and devices [6–16] have also been reported in literature. In addition, a significant amount of work has been reported on defect engineering of its electronic properties [6,7,17–22]. Oxides substrates are also of interest in strain engineering as they offer a variety of lattice parameters.

In many of these applications for $KTaO_3$ and other perovskites, the surface and near-surface structure is important. While strontium titanate is now fairly well understood, and there has been some progress with lanthanum aluminate, little is known about the surfaces of most perovskites including the surface of $KTaO_3$ which is not well understood [23].
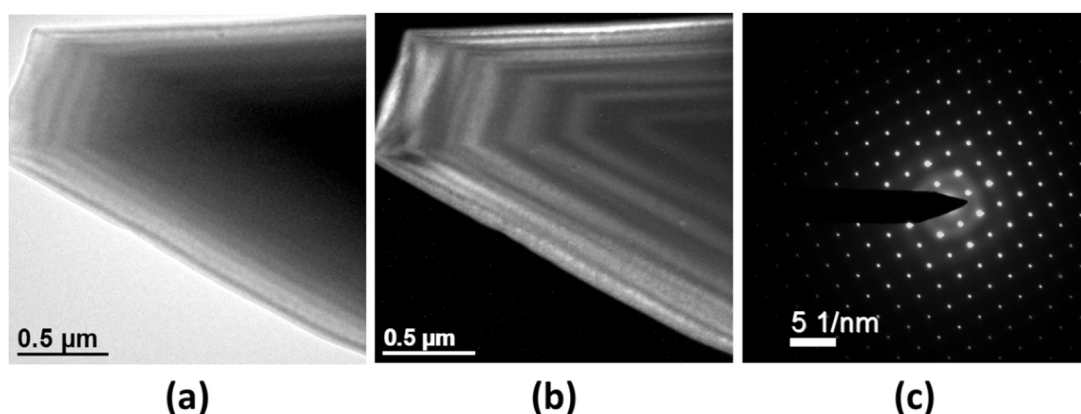

Fig. 1. Bright field and dark field transmission electron microscopy images in (a) and (b) respectively, along with the corresponding transmission electron diffraction pattern in (c) of $KTaO_3$ (001) showing diffuse ring originating from the disordered surface after Ar^+ ion milling.
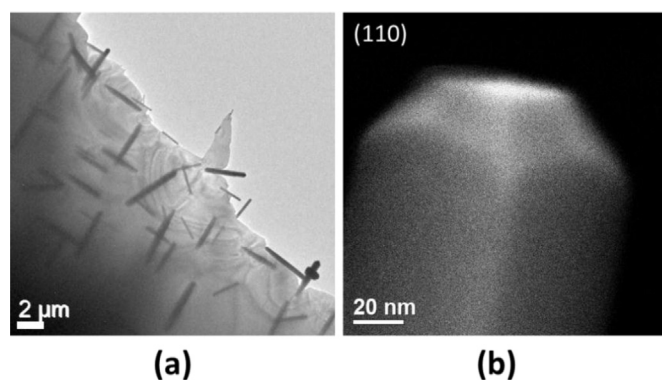
* Corresponding author.
E-mail address: pratikkoirala2017@u.northwestern.edu (P. Koirala).
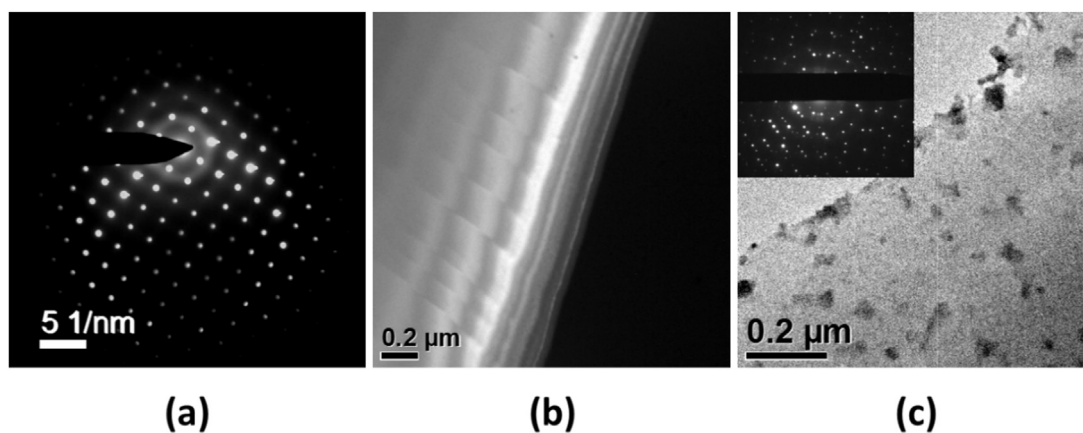
Fig. 2. Off-zone diffraction pattern in (a) of a KTaO$_3$ (001) sample showing disorder of the surface after annealing at 500 °C in flowing oxygen for 10 h. Dark field image of an area of a sample after annealing at 600 °C in (b) showing some order and in (c) area of a sample annealed at 625 °C showing the segregation of a second phase with the corresponding diffraction pattern inset.
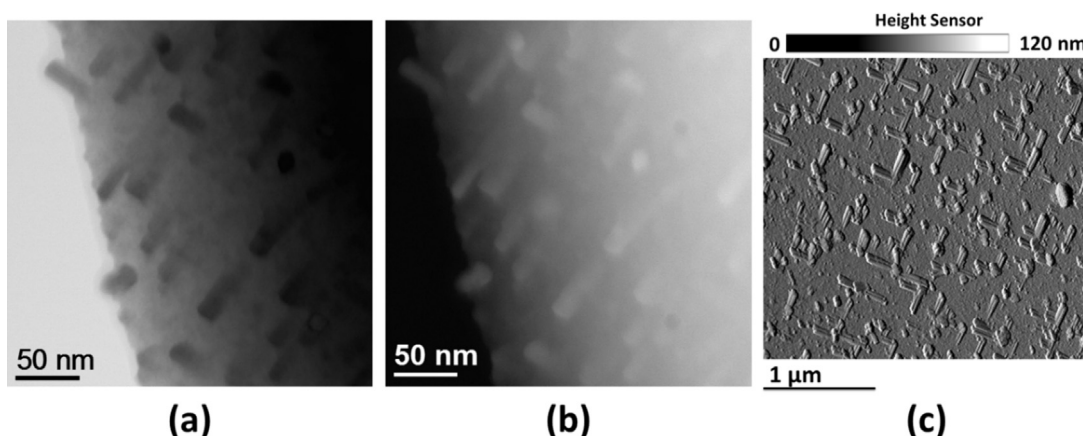
Fig. 3. Bright field and annular dark field image in (a) and (b), respectively, of an area of a sample of KTaO$_3$ (001) after annealing in flowing oxygen for 12 h at 650 °C and atomic force microscopy image in (c) of the same sample (at lower magnification).

Fig. 4. Low magnification image of an area of sample of KTaO$_3$ (001) with second phase after annealing at 650 °C in flowing oxygen for 12 h in (a) and the corresponding secondary electron image of one of the rods of the second phase is in (b) and shows faceted surfaces.

We report here an extensive study of the (001) surface of KTaO$_3$ along with the effect of defect structure on subsequent nucleation of secondary phases. A recent work also reported the precipitation of a tetragonal phase [24], but the origins of the precipitation was not explained. Here we fully explain the origins of such precipitation, and

also devise a preventive measure with a chemical etching approach.

2. Materials and methods

Commercially available single crystalline substrates of (001) oriented KTaO$_3$ were purchased from MTI Corp (Richmond, CA). 3 mm discs were cut using an ultrasonic cutter and mechanically polished to a thickness of ~100 μm with silicon carbide sandpaper and dimpled with a Gatan 656 Dimple Grinder to a thickness of 15μm. Subsequently, the samples were Ar$^+$ ion milled to electron transparency.

Electron microscopy was performed using Hitachi 8100, Hitachi HD-2300, JEOL2100F and JEOL JEM-ARM200CF instruments. Atomic Force Microscopy (AFM) characterization was done using a Bruker FastScan.

3. Results

Electron transparent samples of KTaO$_3$ were first studied using electron microscopy. Viewed along [001], an ion milled sample shows continuous thickness fringes in bright field and dark field images (Fig. 1). The surface suffers from lattice damage and is disordered and amorphous, as seen from the diffuse ring in the diffraction pattern in Fig. 1c.

Lattice damage is commonly observed in ion bombarded samples
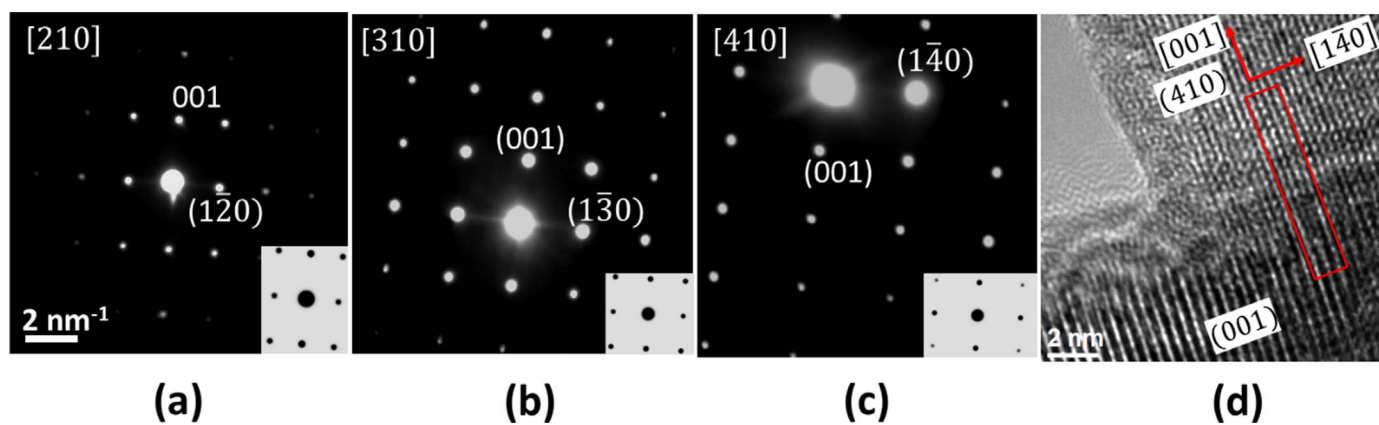
Fig. 5. Transmission electron diffraction pattern along three different orientation (labelled in the top left of each frame) in (a)–(c) and the simulated kinematical diffraction pattern inset for the tetragonal phase – $K_6Ta_{10.8}O_{30}$. The corresponding HREM image in (d) shows the epitaxy between the tetragonal phase and cubic $KTaO_3$. (The red box marks the interface with 4:3 lattice match.). (For interpretation of the references to color in this figure legend, the reader is referred to the web version of this article.)

and there are primarily two methods to clean the surface which involve some combination of chemical etching and annealing. The samples after ion milling were annealed at different temperature in oxidizing conditions to replenish the oxygen content in the material. Samples annealed at 500 °C for 10 h showed an amorphous and disordered surface as indicated by the diffuse ring in the diffraction pattern in Fig. 2a. Increasing the annealing temperature to 600 °C, the surface shows improved crystallinity (see Fig. 2b). However, the surface is not completely flat as one would associate with the formation of steps and terraces which lead to a characteristic contrast in images. On further increase of the annealing temperature to 625 °C, formation of a second phase was observed (see Fig. 2c).

To further understand the surface dynamics and segregation of the secondary phase the samples were subjected to a longer anneal at a higher temperature of 650 °C. This resulted in the nucleation of well-defined nanoparticles on the surface as shown in Fig. 3. Rod shaped precipitates are formed preferentially along the [100] and [010] direction on the cubic substrate, and precipitation occurs only at the surface, i.e. island growth. (Referred here after as islands).

To better define the precipitates they were further annealed for 12 h which led to well faceted, rod shaped islands on the surface (Fig. 4). These islands cover approximately 5–10% of the surface as seen in the low magnification image in Fig. 4a. The islands are well faceted and 2–15 μm long and 20 nm to 1 μm wide.
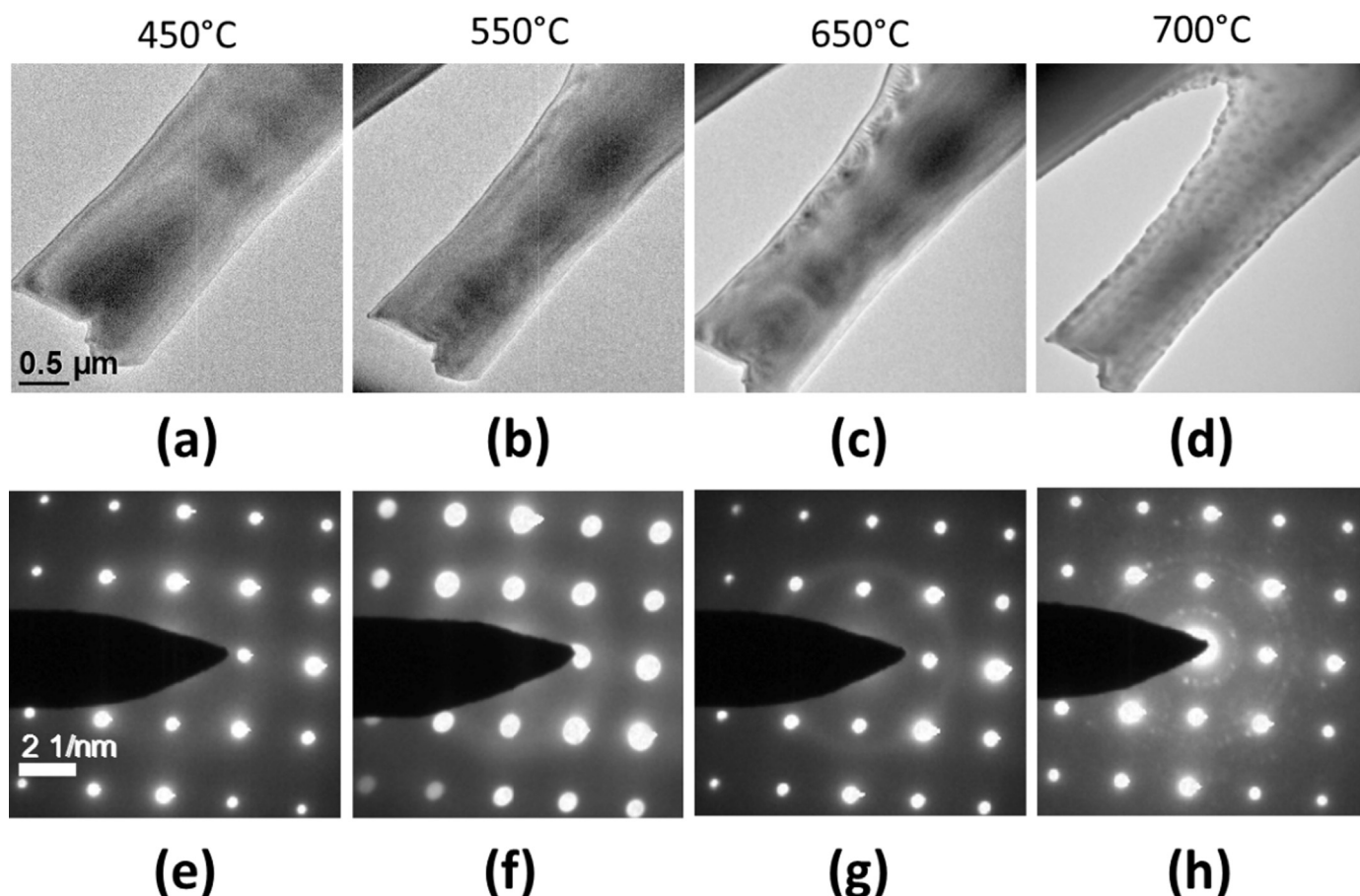
Fig. 6. Bright field TEM images in (a)–(d) from in-situ annealing with the temperature listed on the top of each frame. The corresponding diffraction patterns are given in (e)–(h).
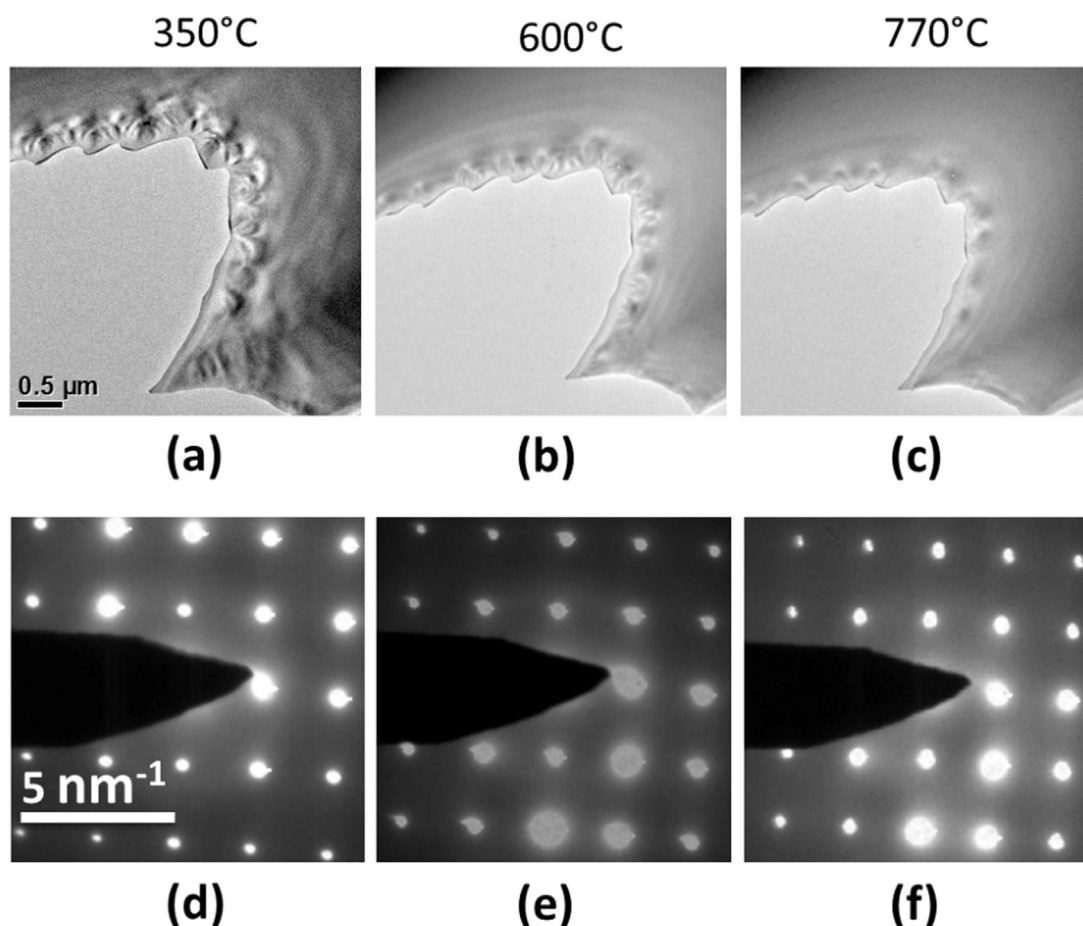
Fig. 7. Bright field TEM images in (a)–(c) from in-situ annealing of BHF etched KTaO3 (001) sample with the temperature listed on the top of each frame. The corresponding diffraction patterns are given in (d)–(f).

To fully establish the phase of these islands, transmission electron diffraction along three different orientations was performed, see Fig. 5. The islands have a tetragonal crystal structure (a=12.569 Å, c=3.978 Å), and Energy Dispersive X-ray Spectroscopy (EDS) indicated that the precipitates are K deficient (12–14 at%) and rich in oxygen (70–72 at%) and Tantalum (21–23 at%). This is again consistent with the tetragonal phase, $K_6Ta_{10.8}O_{30}$ [25].

The in-plane orientation of the tetragonal phase is along [1$\bar{3}$0]/[001] with good in plane lattice match with the cubic phase of $KTaO_3$.

The origins of precipitation and the mechanism were investigated by heating the samples in-situ in an electron microscope. Four TEM images along with the corresponding diffraction patterns are given in Fig. 6 and the temperature is listed at the top of each frame. We note that this temperature is at the heater and the effective temperature at the sample is expected to be lower. The frames show continuous changes in strain contrast with increasing temperature and when the temperature reaches 700 °C, there is precipitation of islands on the surface.

The second phase segregates relieving the strain and reaching a thermodynamic equilibrium in surface stoichiometry, interfacial and surface energies, with some vaporization of KO_x which has a vapor pressure of 10^{-9} bar at 600 °C [26] and atmospheric pressure. The rings in diffraction pattern from the second phase show spacings consistent with the tetragonal phase as discussed earlier.

Buffered HF etch is often used to etch oxides crystal for creating a crystalline surfaces and also to create a specific termination, and has reported for $KTaO_3$ to create atomically flat surfaces with unit cell steps [27].

Ion milled samples were etched with BHF and then subjected to in-situ heating in electron microscopy to compare the differences in surface morphology and segregation of the secondary phase on the surface with the as prepared sample. The TEM images given in Fig. 7 along with the corresponding diffraction pattern show gradual strain relief without the formation of the secondary phase even at temperatures much higher than when the second phase was observed on the as ion milled samples. This validate that the surface disorder in ion milled samples is the cause for the nucleation of second phase on the surface on annealing.

4. Conclusion

Surface heterogeneity in oxides and other binary compounds is a general phenomenon. These usually result due to the two steps involved in processing these samples: ion milling and annealing. Ar^+ ion milling is widely used to create thin samples for electron microscopy or to clean samples. However, the energies used in ion milling (2–6 keV) is detrimental to the surface stoichiometry and creates defects and disorder. These defects are usually eradicated by etching or annealing techniques. However, the choice of etchant and annealing conditions will vary depending upon the material. The two different in-situ annealing experiments reported in this paper demonstrate the role of surface disorder and off-stoichiometry on the resulting secondary phase that precipitates. EDS results indicate depletion of potassium, whereas the ratio of tantalum to oxygen remains approximately the same as in $KTaO_3$ indicating that the ordering of the secondary phase is mostly guided by the deficiency of K which could result from either selective sputtering of K during ion milling or due to the evaporation of K in the form of an oxide.

References

[1] R.G. Geyer, B. Riddle, J. Krupka, L.A. Boatner, Microwave dielectric properties of single-crystal quantum paraelectrics KTaO3 and SrTiO3 at cryogenic temperatures, J. Appl. Phys. 97 (2005) 104111.

[2] K. Zou, S. Ismail-Beigi, K. Kisslinger, X. Shen, D. Su, F.J. Walker, C.H. Ahn, LaTiO$_3$/KTaO$_3$ interfaces: a new two-dimensional electron gas system, APL Mater. 3 (2015) 036104.

[3] T. Ishihara, H. Nishiguchi, K. Fukamachi, Y. Takita, Effects of acceptor doping to KTaO$_3$ on photocatalytic decomposition of pure H$_2$O, J. Phys. Chem. B 103 (1999) 1–3.

[4] H. Hayashi, Y. Hakuta, Hydrothermal epitaxy of KTaO$_3$ thin films under super-critical water conditions, J. Mater. Sci. 43 (2007) 2342–2347.

[5] M. Marchelek, B. Bajorowicz, P. Mazierski, A. Cybula, T. Klimczuk, M. Winiarski, N. Fijałkowska, A. Zaleska, KTaO$_3$-based nanocomposites for air treatment, Catal. Today 252 (2015) 47–53.

[6] O. Aktas, S. Crossley, M.A. Carpenter, E.K.H. Salje, Polar correlations and defect-induced ferroelectricity in cryogenic KTaO3, Phys. Rev. B 90 (2014).

[7] W.S. Baer, Faraday rotation in KTaO$_3$, Phys. Rev. Lett. 16 (1966) 729–731.

[8] W.R. Hosler, H.P.R. Frederikse, Magnetoresistive effects in KTaO$_3$, Solid State Commun. 7 (1969) 1443–1449.

[9] K.W. Johnson, D.H. Olson, Electron tunneling into KTaO$_3$ Schottky Barrier Junctions, Phys. Rev. B 3 (1971) 1244–1248.

[10] P. Kim, K.T. Kang, G. Go, J.H. Han, Nature of orbital and spin Rashba coupling in the surface bands of SrTiO$_3$ and KTaO$_3$, Phys. Rev. B 90 (2014).

[11] G. Shirane, R. Nathans, V.J. Minkiewicz, Temperature dependence of the soft ferroelectric mode in KTaO$_3$, Phys. Rev. 157 (1967) 396–399.

[12] V. Skoromets, C. Kadlec, H. Němec, D. Fattakhova-Rohlfing, P. Kužel, Tunable dielectric properties of KTaO$_3$ single crystals in the terahertz range, J. Phys. D: Appl. Phys. 49 (2016) 065306.

[13] S. Triebwasser, Study of ferroelectric transitions of solid-solution single crystals of KNbO$_3$-KTaO$_3$, Phys. Rev. 114 (1959) 63–70.

[14] K. Ueno, I.H. Inoue, T. Yamada, H. Akoh, Y. Tokura, H. Takagi, Field-effect transistor based on KTaO$_3$ perovskite, Appl. Phys. Lett. 84 (2004) 3726.

[15] L. Wu, H. Li, L. Jiang, C. Ding, Q. Sheng, X. Ding, J. Yao, Modulation of dielectric properties of KTaO$_3$ in terahertz region via 532 nm continuous-wave laser, Opt. Mater. Express 4 (2014) 2595.

[16] Y. Yang, C.-S. Lin, J.-F. Chen, L. Hu, W.-D. Cheng, Ferromagnetic-nonmagnetic and metal-insulator phase transitions at the interfaces of KTaO$_3$ and PbTiO$_3$, J. Appl. Phys. 116 (2014) 153709.

[17] V.V. Laguta, M.D. Glinchuk, I.P. Bykov, A. Cremona, P. Galinetto, E. Giulotto, L. Jastrabik, J. Rosa, Light-induced defects in KTaO$_3$, J. Appl. Phys. 93 (2003) 6056.

[18] G.O. Deputy, R.W. Vest, Defect structure and electrical properties of KTaO$_3$, J. Am. Ceram. Soc. 61 (1978) 321–325.

[19] X. Liu, J. Lv, S. Wang, X. Li, J. Lang, Y. Su, Z. Chai, X. Wang, A novel contractive effect of KTaO$_3$ nanocrystals via La3+ doping and an enhanced photocatalytic performance, J. Alloy. Compd. 622 (2015) 894–901.

[20] A. Sakai, T. Kanno, S. Yotsuhashi, H. Adachi, Y. Tokura, Thermoelectric properties of electron-doped KTaO$_3$, Jpn. J. Appl. Phys. 48 (2009) 097002.

[21] B. Salce, J.L. Gravil, L.A. Boatner, Disorder and thermal transport in undoped KTaO$_3$, J. Phys.: Condens. Matter 6 (1994) 4077–4092.

[22] M. Dubus, B. Daudin, B. Salce, L.A. Boatner, Ion channeling studies of KTaO$_3$:nb, Solid State Commun. 55 (1985) 759–763.

[23] J.A. Li, E.A. Akhadov, J. Baker, L.A. Boatner, D. Bonart, J. Fritsch, S.A. Safron, U. Schröder, J.G. Skofronick, T.W. Trelenberg, Surface structure and dynamics of KTaO$_3$(001), Phys. Rev. B 68 (2003).

[24] Y.B. Xu, Y.L. Tang, Y. Liu, X.L. Ma, Y.L. Zhu, Atomically resolved precipitates/matrix interfaces in KTaO$_3$ crystals, Philos. Mag. 96 (2016) 486–497.

[25] A.A. Awadalla, B.M. Gatehouse, Crystal structures of some niobium and tantalum oxides. III K6Ta10.8O30—a partially "Filled" tetragonal tungsten bronze-like structure, J. Solid State Chem. 23 (1978) 349–355.

[26] R.H. Lamoreaux, D.L. Hildenbrand, High temperature vaporization behavior of Oxides. I. Alkali metal binary oxides, J. Phys. Chem. Ref. Data 13 (1984) 151.

[27] H.-j Bae, J. Sigman, D.P. Norton, L.A. Boatner, Surface treatment for forming unit-cell steps on the (001) KTaO$_3$ substrate surface, Appl. Surf. Sci. 241 (2005) 271–278.